19th Australasian Fluid Mechanics Conference
Melbourne, Australia
8-11 December 2014

Numerical Simulation of a Rough-Wall Pipe from the Transitionally Rough Regime to the Fully Rough Regime

L. Chan, M. MacDonald, D. Chung, N. Hutchins and A. Ooi

Department of Mechanical Engineering
University of Melbourne, Victoria 3010, Australia

Abstract

Turbulent flow of a rough-wall pipe is simulated using Direct Numerical Simulations (DNS) at low and medium Reynolds number from the transitionally rough regime to the fully rough regime. The rough surfaces simulated consist of three-dimensional sinusoidal roughness elements. The size of the roughness (roughness semi-amplitude height h^+ and wavelength λ^+) is increased geometrically while maintaining the height-to-wavelength ratio of the sinusoidal roughness element. A method is developed to accurately calculate the roughness function ΔU^+ for the simulations conducted at low Reynolds number. For this surface, the flow is fully rough when $h^+ \approx 60$ (simulated at $Re_\tau = 540$). This corresponds to $k_s^+ \approx 4.1h^+$ where k_s^+ is Nikuradse's equivalent sandgrain roughness. A linear trend is observed when the ratio of the apparent wall shear stress due to form drag on the roughness elements to the total wall shear stress $R_\tau = \tau_R/\tau_T$ is plotted against the log of the roughness height h^+. This linear trend is also observed in the transitionally rough regime. For all the rough-wall pipe simulations conducted, Townsend's [15] outer layer similarity hypothesis holds true.

Introduction

Rough wall-bounded turbulent flow has been extensively investigated due to its many practical applications. Being able to predict the drag caused by a given rough surface (i.e the surface of a ship's hull or aircraft fuselage) is critical to predicting the propulsive requirements for many engineering system. The current state of the art for predicting the drag increment due to a given surface is to conduct scaled experiments. Replicas of engineering surfaces are geometrically scaled and tested in a laboratory facility to determine the influence of the roughness on the flow (for example the turbine blade roughness investigated by [16, 9]). Typically the equivalent sandgrain roughness k_s is used as the standard measure in determining how rough the surface is. These results can subsequently be used to predict the full-scale performance of the surface. Conducting such experiments in the laboratory is time consuming and expensive, and ideally it would be preferable to be able to predict k_s directly from the physical characteristics of the rough surface. In the biomedical field, it is found that turbulence can occur in blood flow (due to pathological conditions or in the descending aorta) and its physiological effects are of medical interest.

With the advancement of computing power, Computational Fluid Dynamics (CFD) is becoming an important tool in understanding wall bounded turbulent flows. It is now becoming increasingly feasible to simulate flows at higher Reynolds numbers and to compute more complex roughness geometries. In this paper, a turbulent flow through a rough-wall pipe is simulated from the transitionally rough to the fully rough regime. The roughness elements of the pipe consist of three dimensional sinusoidal roughness. Current work is inspired by [14] and [13] who carried out experiments on a honed rough pipe and on a rough boundary layer (where the roughness was geometrically similar to the honed pipe) respectively. In these studies, the flow varies from the hydraulically smooth to the fully rough regime by changing the Reynolds number of the flow, which effectively increases the roughness Reynolds number $k_s^+ = k_s U_\tau/\nu$ while maintaining the physical size of the roughness. For the roughness cases simulated in this paper, the roughness elements will be geometrically scaled and simulated at $Re_\tau = 180$ and 540.

Throughout this paper, cylindrical coordinates are used where r is the radial direction (measured from the centre of the pipe), θ is the azimuthal angle, x is in the streamwise direction and the arc length $s = r\theta$. Capitalised variables (e.g., U_τ) indicate time- and spatially-averaged quantities and the '+' superscript is used to denote viscous scalings of length ($r^+ = rU_\tau/\nu$), velocity ($u^+ = u/U_\tau$) and time ($t^+ = tU_\tau^2/\nu$).

Numerical Procedure

The turbulent flow through a pipe is solved using the Navier-Stokes equations for incompressible flow in Cartesian coordinates:

$$\nabla \cdot \mathbf{u} = 0, \tag{1a}$$

$$\frac{\partial \mathbf{u}}{\partial t} + \mathbf{u}\cdot\nabla\mathbf{u} = -\frac{1}{\rho}\nabla p + \nu\nabla^2\mathbf{u} + F_x\mathbf{i}, \tag{1b}$$

where $\mathbf{u} = (u, v, w)$ is the velocity in the x, y, and z directions, t is time and $F_x(t)$ is the uniform, time-varying body force required to maintain a constant mass flux through the pipe. The code used for this simulation is CDP, a finite-volume unstructured-grid code [5, 8]. The diffusive and convective terms are advanced in time using the second-order, fully-implicit Crank-Nicolson scheme. and continuity is enforced by the fractional-step method by [7]. A Cartesian 'O-grid' mesh is used for the simulations instead of a cylindrical polar mesh as it allows for better control of the number of grid points in the azimuthal direction, which is fixed for a cylindrical polar mesh at all wall normal distances. The grid is uniformly spaced in the streamwise direction and a linear expansion is used in the radial direction to ensure sufficient resolution at the wall of the pipe. At the centre of the pipe, the cells are sized to be approximately cube shaped ($\Delta r^+ \approx \Delta r\theta^+ \approx \Delta x^+$). Computational details regarding the mean grid spacing near the wall for each case are given in table 1. It is important to highlight that for cases 02_018 and 05_035, there are only 4 and 8 grid points per roughness wavelength and hence the topological features of the sinusoidal surface are not fully resolved (a more faceted version of the roughness is effectively simulated).

The no-slip condition is applied to the walls of the pipe and a periodic boundary condition is applied to the ends of the pipe. The length of the pipe is selected to be $L_x = 4\pi R_0$ where R_0 is the reference radius. The domain length used is longer than the domain used by [4] which had a length of $10R_0$. According to [2] who conducted a domain length study, for a turbulent pipe flow, the velocity and turbulence intensity profiles are converged when $L_x = 4\pi R_0$.

The flow of the smooth wall pipe at $Re_\tau = 180$ was initialised

Case	$N_{r,\theta}$	N_x	N_{λ_x}	Δr^+	Δx^+
	$Re_\tau = 180$				
Smooth	13685	384	-	0.33	6.1
02_018	24864	512	4	0.12	3.5
05_035	24864	512	8	0.12	3.4
10_070	24864	512	16	0.11	3.2
13_094	24864	512	21	0.11	3.3
16_113	24864	512	26	0.16	3.2
20_141	19872	512	32	0.11	3.2
	$Re_\tau = 540$				
Smooth	94752	1152	-	0.23	5.8
20_141	104400	1152	24	0.14	4.4
40_283	104400	1152	48	0.13	4.1
60_424	108720	1152	72	0.15	4.0
80_565	108720	1152	96	0.14	3.8

Table 1. Computational details of the meshes used for $Re_\tau = 180$ and 540 simulations. $N_{r,\theta}$ is the number of elements in an (r,θ) plane, N_x the number of elements in the streamwise direction and N_{λ_x} the number of elements per roughness wavelength. Δr^+ and $\Delta z^+ \approx \Delta r\theta^+$ are the mean grid spacings in wall-units at the wall calculated using the local U_τ. The largest cells are located at the centre of the pipe where $\Delta r^+ \approx \Delta r\theta^+ \approx \Delta x^+$.

using a parabolic curve with random fluctuations added. As noted by [4], due to the low Reynolds number of the flow, the random fluctuations can cause significant viscous dissipation and hence relaminarisation of the flow. Therefore, a smaller viscosity was temporarily used to allow the perturbations to grow into turbulent fluctuations. This regime was run for 2500 timesteps with an initial timestep of $\Delta t^+ = 0.036$ to ensure stability. The timestep was progressively increased until a value of $\Delta t^+ = 0.144$, where the Courant-Friedrichs-Lewy (CFL) number was approximately 0.8. The viscosity was also progressively increased during the same period. The simulation is then run for $30T$ (where $T = L_x/U_b$ is the flow-through time based on bulk velocity) for the flow to become independent of any initial transients before gathering statistics of the flow field. The rough wall simulations are initialised by interpolating the flow-field of the developed smooth-wall pipe case. Again, a small timestep and viscosity were initially used and slowly increased until reaching a timestep of $\Delta t^+ = 0.07$. For the $Re_\tau = 540$ cases, the timestep used for the smooth and rough cases are $\Delta t^+ = 0.09$ and $\Delta t^+ = 0.05$ respectively. Data is collected every $500\Delta t^+$ and the simulation is run for $20T$ for the $Re_\tau = 180$ cases and $5T$ for the $Re_\tau = 540$ cases to obtain well-converged statistics.

The rough surface of the simulated pipe R is described by a cosine function as given by,

$$R(x,\theta) = R_0 + h\cos\left(\frac{2\pi x}{\lambda_x}\right)\cos\left(\frac{2\pi R_0\theta}{\lambda_s}\right) \tag{2}$$

where the reference radius of the pipe R_0, is set to be the mean radius of the pipe $\overline{R}$, h is the semi-amplitude of the sinusoidal roughness (half of the peak-to-trough height $k_t = 2h$) and λ_x and λ_s are the wavelengths of the roughness elements in the streamwise and azimuthal directions respectively. For all of the rough cases, $\lambda_x = \lambda_s$ and has a roughness semi-amplitude to wavelength ratio of $h/\lambda_x = 0.141$. All the roughness elements have a root-mean-square roughness height that is twice the roughness semi-amplitude $k^+_{rms} = 2h^+$ and an effective slope ES (defined in [10] as the mean of the absolute streamwise gradient) of 0.361. However, for case 02_018 and 05_035, ES is underestimated (10% less for case 02_018) due to the insufficient number of grid points per roughness element.

Throughout the paper, the roughness cases are identified by the following identifying code

$$\underbrace{\boxed{1}\boxed{0}}_{h^+} - \underbrace{\boxed{1}\boxed{4}\boxed{1}}_{\lambda^+} \tag{3}$$

where the first two digits represent the roughness semi-amplitude and the last three digits represent the streamwise or spanwise wavelength of the roughness elements (both in viscous units). In this paper, the roughness elements are geometrically scaled for roughness semi-amplitude values of $h^+ = 2.5, 5, 10, 13.3, 16$ and 20 at $Re_\tau = 180$ and for $h^+ = 20, 40, 60$ and 80 at $Re_\tau = 540$.

Mean Velocity Profile

The roughness elements causes a downward shift in the mean streamwise velocity profile when scaled in viscous units. This shift is measured by the roughness function ΔU^+ in the modified logarithmic law [6],

$$U^+ = \frac{1}{\kappa}\ln(y^+) + C - \Delta U^+ \tag{4}$$

where we assume $\kappa = 0.4$ and $C = 5.3$ for current simulations. The value of C used is 0.1 lower than the value used by [1] who conducted numerical simulations at a lower Reynolds number ($Re_\tau = 314$). Figure 1(a,d) illustrates the mean streamwise velocity profile of the flow at $Re_\tau = 180$ and 540 respectively. The smooth profiles are coloured in black while the rough profiles are shaded grey, where surfaces with larger roughness elements have lighter shades of grey. It can be seen that increasing the roughness size causes a downward shift in the mean velocity profile (as illustrated by the arrows). However, when plotting the velocity defect profiles (see figure 1(b,e)), a remarkable collapse is obtained in the outer layer of the flow with all the rough profiles (at $Re_\tau = 180$ and 540) falling on the smooth profile for values of $y/R_0 > 0.2$. Interestingly, this collapse is also obtained for the largest roughness element which has a reference radius to roughness height ratio h/R_0 of 0.148. This observation is consistent with Townsend's outer-layer similarity hypothesis [15] which states that the turbulence at the outer region of the flow is independent of the 'roughness' when scaled with the roughness value of U_τ. To quantify the effects of the roughness on the flow (particularly in higher Re applications), the roughness function ΔU^+ has to be measured accurately. ΔU^+ is measured from the log region of the flow for cases at $Re_\tau = 540$. However, at $Re_\tau = 180$, the log region of the flow, which is traditionally assumed to lie between $30 < y^+ < 0.15\delta^+$ (where the boundary layer thickness δ^+ is equvalent to the reference radius R_0^+ in a pipe), is poorly defined due to the low Reynolds number. Figure 1(c,f) illustrates for the $Re_\tau = 180$ and 540 cases respectively the mean velocity profile expressed in the correction constant form $C - \Delta U^+ = U^+ - (1/\kappa)\ln(y^+)$. Under this representation, the log region in the flow would appear to be a horizontal plateau. In figure 1(f) the horizontal dashed line coincides with the simulated cases while in figure 1(c), this region is not observed as the profiles have a higher slope. Since the log region of the $Re_\tau = 180$ simulations is ill-defined, the centreline mean velocity is used to calculate ΔU^+.

Transitionally Rough Regime to Fully Rough Regime

The roughness function are plotted in figure 2 against the equivalent sand grain roughness k_s^+. The flow, which is initially in the transitionally rough regime, approaches the fully rough regime as the size of the viscously scaled roughness elements increases. For $h^+ > 60$, the flow is in the fully rough regime since the variation of ΔU^+ with k_s^+ falls on to the fully rough asymptote. Note that if we assume Nikuradse's constant $B = 8.5$, this

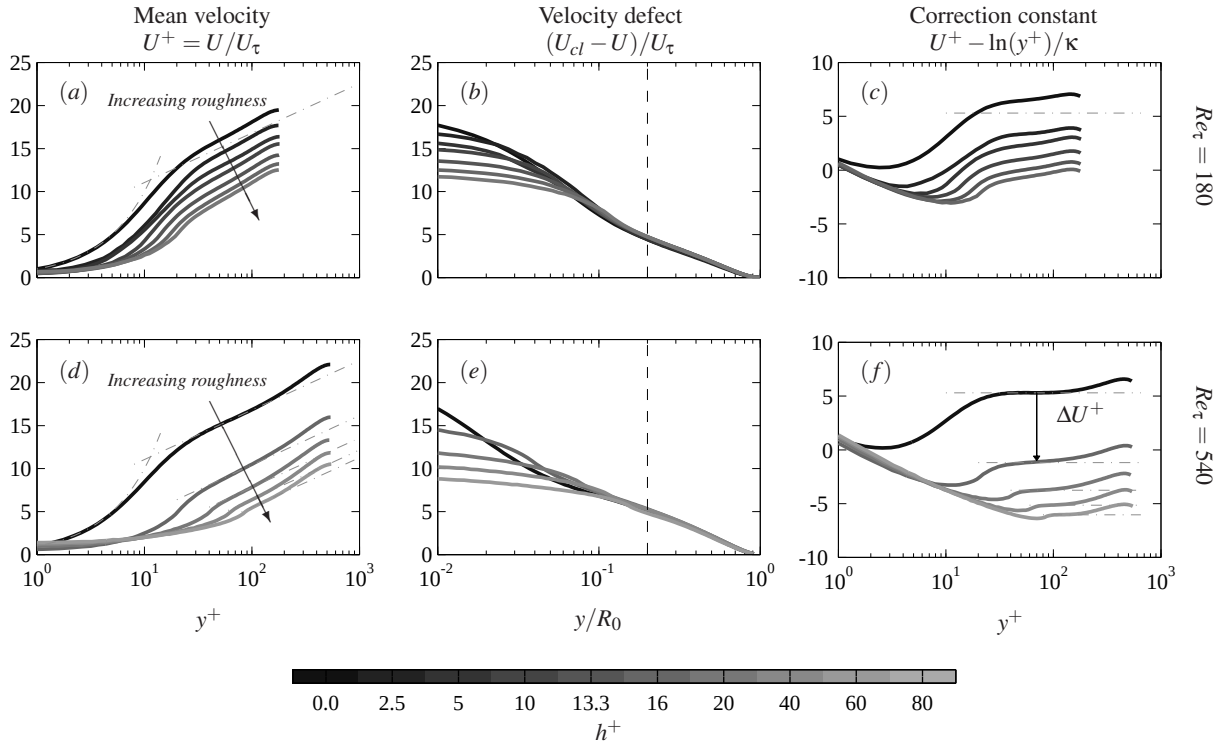

Figure 1. Mean streamwise velocity profile for the various roughness cases simulated at $Re_\tau = 180$ (top) and $Re_\tau = 540$ (bottom) in three different forms. The mean streamwise velocity profile against the viscous wall normal location (a,d), the velocity defect (b,e) and the correction constant (c,f). Dash-dotted lines in (a) and (d) show $U^+ = y^+$ and $U^+ = (1/\kappa)\log(y^+) + C$, where $\kappa = 0.40$ and $C = 5.3$ while dash line in (b) and (e) is at $y/R_0 = 0.2$. Roughness semi-amplitude $h^+ = 2.5, 5, 10, 13, 16$ and 20 are simulated at $Re_\tau = 180$ and $h^+ = 20, 40, 60$ and 80 are simulated at $Re_\tau = 540$

suggests that $k_s^+ = 4.1h^+$. The three-dimensional sinusoidal roughness reaches the fully rough asymptote when $k_s^+ \approx 180$– a value far greater than the one obtained by Nikuradse's sand grain roughness ($k_s^+ \approx 40$) [11]. One possible reason why Nikuradse's rough surface approaches the fully rough asymptote faster than our simulated roughness is because of the sharp edges of the sandgrain roughness causes the flow to separate at smaller values of k_s^+. When flow separation occurs, the pressure drag acting on the rough surface increases. Colebrook's 'universal' roughness function [3] (shown by the solid line on figure 2) overestimates ΔU^+ for sandgrain and three-dimensional sinusoidal roughness elements in the transitionally rough regime and is therefore considered to be conservative.

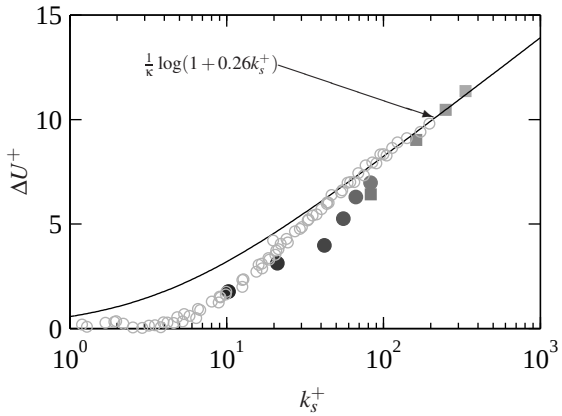

Figure 2. Roughness function ΔU^+ against equivalent sandgrain roughness k_s^+. Circle symbols are simulated at $Re_\tau = 180$ and square symbols are simulated at $Re_\tau = 540$. Solid line: Colebrook 'universal' roughness function [3]. Open circles: Nikuradse sandgrain roughness function [11].

It is important to note that there are differences in ΔU^+ for the case with roughness height $h^+ = 20$ when simulated at two different Reynolds number ($Re_\tau = 180$ and 540). The differences are due to the low Reynolds number effect which is more prominently observed in the smooth case (steeper 'log' region) than in the rough case at $Re_\tau = 180$ (see figure 3). The higher centreline mean velocity of the smooth wall causes the overestimation of ΔU^+ by about 0.7. A better method to calculate ΔU^+ would be to compare the mean velocity profile of the rough-wall at $Re_\tau = 180$ with the log-law. While this method would lead to a better estimation of ΔU^+ for case 20_141, it could potentially result in negative values of ΔU^+ for very small roughnesses. Overall, the discrepancy in ΔU^+ is small and for engineering type applications, the difference in the calculated coefficient of friction C_f would be less than 5%.

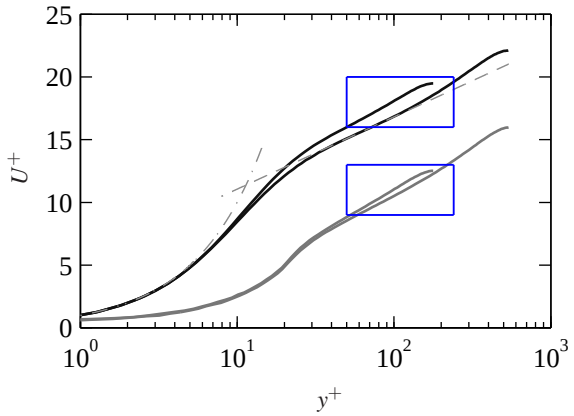

Figure 3. Mean velocity profile for the smooth case and 20_141 at $Re_\tau = 180$ and 540. Blue box highlights the differences between the simulations conducted at different Reynolds number.

In the fully rough regime, it is often assumed that the pressure drag dominates the viscous drag in the flow. This was demonstrated by [12], who conducted rough pipe experiments on hemispheres and cones finding that in a fully rough flow, the ratio of the apparent wall shear stress due to form drag on the roughness elements to the total wall shear stress $R_\tau = \tau_R/\tau_T$ is

at least 0.8. To assess this finding, the ratio between the pressure drag to the total drag is plotted against the roughness height h^+ in figure 4. For the current sinusoidal roughness simulated, the flow is fully rough when $R_\tau \approx 0.75$. An interesting observation from figure 4 is that R_τ increases approximately linearly with the log of h^+ even in the transitionally rough regime. From our linear curve fit, $R_\tau = 0.14\log(h^+) + 0.15$, we obtain $h^+ = 433$ when $R_\tau = 1$ and $h^+ = 0.34$ ($k_s^+ \approx 1.33$) when $R_\tau = 0$, which seems to be reasonable estimates at the limits of R_τ. It is also important to highlight that R_τ for case 20_141 at $Re_\tau = 180$ and 540 is roughly the same despite having different ΔU^+ as mentioned previously.

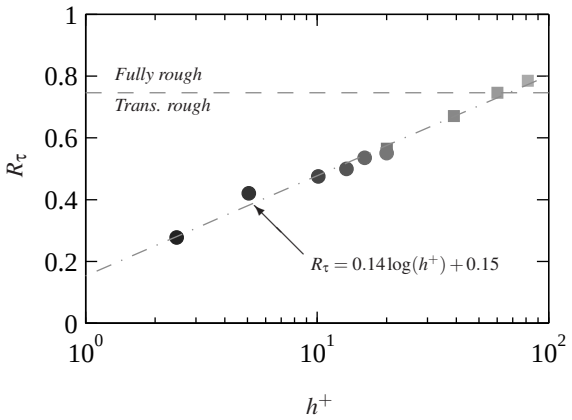

Figure 4. The ratio of the apparent wall shear stress due to form drag on the roughness elements to the total wall shear stress $R_\tau = \tau_R/\tau_T$ against roughness height h^+.

Conclusion

Direct numerical simulation is simulated at $Re_\tau = 180$ and 540 over a three-dimensional sinusoidal roughness where the flow ranges from the transitionally rough regime to the fully rough regime. The low Reynolds number simulations at $Re_\tau = 180$ provides a reasonable estimate of ΔU^+, which is attractive for engineering applications as it is computationally cheap. For the roughness geometry simulated, the flow approaches the fully rough asymptote at a much larger k_s^+ than Nikuradse's sand grain roughness [11]. A slightly higher ΔU^+ is obtained when the viscously scaled roughness (case 20_141) is simulated at $Re_\tau = 180$ than the simulation at $Re_\tau = 540$ due to the low Reynolds number effect of the flow. For the range of cases simulated, an approximately linear trend is obtained when R_τ is plotted against the log of h^+.

Acknowledgements

The authors would like to gratefully thank the financial support of the Australian Research Council (ARC) and the computational time granted under the Resource Allocation Scheme by the Victorian Life Science Computational Institute (VLSCI).

References

[1] Blackburn, H. M., Ooi, A. and Chong, M. S., The effect of corrugation height on flow in a wavy-walled pipe, in *16th Australasian Fluid Mechanics Conference*, Gold Coast, Australia, 2007.

[2] Chin, C., Ooi, A. S. H., Marusic, I. and Blackburn, H. M., The influence of pipe length on turbulence statistics computed from direct numerical simulation data, *Phys. Fluids*, **22**, 2010, 115107.

[3] Colebrook, C. F., Turbulent flow in pipes, with particular reference to the transition region between the smooth and rough pipe laws., **11**, 1939, 133–156.

[4] Eggels, J. G. M., Unger, F., Weiss, M. H., Westerweel, J., Adrian, R. J., Friedrich, R. and Nieuwstadt, F. T. M., Fully developed turbulent pipe flow: A comparison between direct numerical simulation and experiment, *J. Fluid Mech.*, **268**, 1994, 175–209.

[5] Ham, F. and Iaccarino, G., Energy conservation in collocated discretization schemes on unstructured meshes, in *Annual Research Briefs 2004*, Center for Turbulence Research Stanford University/ NASA Ames, 2004.

[6] Hama, F. R., Boundary-layer characteristics for smooth and rough surfaces, *Trans. Soc. Naval Archit. Mar. Eng.*, **62**, 1954, 333–358.

[7] Kim, J. and Moin, P., Application of a fractional-step method to incompressible navier-stokes equations, *J. Comput. Phys.*, **59**, 1985, 308–323.

[8] Mahesh, K., Constantinescu, G. and Moin, P., A numerical method for large-eddy simulation in complex geometries, *J. Comput. Phys.*, **197**, 2004, 215–240.

[9] Mejia-Alvarez, R. and Christensen, K. T., Low-order representations of irregular surface roughness and their impact on a turbulent boundary layer, *Phys. Fluids*, **22**, 2010, 015106.

[10] Napoli, E., Armenio, V. and De Marchis, M., The effect of the slope of irregularly distributed roughness elements on turbulent wall-bounded flows, *J. Fluid Mech.*, **613**.

[11] Nikuradse, J., *Laws of flow in rough pipes*, National Advisory Committee for Aeronautics Washington, 1933.

[12] Scaggs, W. F., Taylor, R. P. and Coleman, H. W., Measurement and prediction of rough wall effects on friction factoruniform roughness results, *J. Fluids Eng.*, **110**, 1988, 385–391.

[13] Schultz, M. P. and Flack, K. A., The rough-wall turbulent boundary layer from the hydraulically smooth to the fully rough regime, *J. Fluid Mech.*, **580**, 2007, 381–405.

[14] Shockling, M. A., Allen, J. J. and Smits, A. J., Roughness effects in turbulent pipe flow, *J. Fluid Mech.*, **564**, 2006, 267–285.

[15] Townsend, A. A., *The structure of turbulent shear flow*, Cambridge University Press, 1980.

[16] Wu, Y. and Christensen, K. T., Outer-layer similarity in the presence of a practical rough-wall topography, *Phys. Fluids*, **19**, 2007, 085108.